An Optimization-Based Approach to the HYRMAN Manipulator's Inverse Kinematics

Francesca Pagano, Mario Selvaggio, Vincenzo Lippiello, and Bruno Siciliano

Abstract This work presents an optimization-based approach to solve the inverse kinematics problem of HYRMAN, a hyper-redundant manipulator designed for remote maintenance of nuclear fusion reactors. The proposed redundancy resolution method executes multiple prioritized tasks, namely end-effector trajectory tracking, joint limit avoidance, collision avoidance, torque and length minimization, and convergence to the torus center. Set-based and secondary tasks are encoded with control barrier functions within a quadratic optimization problem that can be solved online. Numerical simulations illustrate task execution and the capability to retract from the vessel through the tokamak's port duct.

F. Pagano
Centro Servizi Metrologici e Tecnologici Avanzati (CeSMA), University of Naples Federico II, Corso Nicolangelo Protopisani, 80146, Napoli, Italy
e-mail: francesca.pagano@unina.it

M. Selvaggio
Department of Electrical Engineering and Information Technology, University of Naples Federico II, Via Claudio 21, 80125, Napoli, Italy
e-mail: mario.selvaggio@unina.it

V. Lippiello
Department of Electrical Engineering and Information Technology, University of Naples Federico II, Via Claudio 21, 80125, Napoli, Italy
e-mail: vincenzo.lippiello@unina.it

B. Siciliano
Department of Electrical Engineering and Information Technology, University of Naples Federico II, Via Claudio 21, 80125, Napoli, Italy
e-mail: bruno.siciliano@unina.it

1 Introduction

Hyper-redundant manipulators are commonly employed in remote operations within confined environments, where a high number of degrees of freedom (DoFs) is essential to achieve sufficient maneuverability and dexterity. A notable example is HYRMAN, a manipulator designed for remote handling (RH) operations in the Divertor Tokamak Test (DTT) nuclear fusion reactor, and currently being manufactured by OCIMA[1]. This robotic arm shall handle the first wall (FW) modules and the Ion Cyclotron Heating antennas of DTT, which are accessible only through dedicated port ducts, and carry payloads up to 350 kg with a positioning accuracy of 10 mm/2°. Thanks to its hyper-redundancy, dedicated algorithms can address application-specific constraints, such as those imposed by the narrow entrance and the high payload. This work addresses these objectives by proposing a solution to the HYRMAN's inverse kinematic problem to optimally map assigned task-space variables (e.g., end-effector pose) to corresponding joint configurations. This correspondence can be derived by inverting the direct kinematics function, employing Jacobian-based closed-loop algorithms [6], or resorting to local or global optimization methods [3]. Previous works on similar kinematic structures have adopted analytical approaches, selecting the most suitable solution according to predefined rules [9], or hybrid strategies that combine analytical and optimization methods in two separate modules [4, 2]. Our approach formulates a single quadratic optimization (QP) problem to solve the inverse kinematics of the entire manipulator. Control barrier functions (CBFs) are used in the QP to encode both safety constraints and secondary objectives, thereby satisfying operational requirements, including the retraction of the arm within the port duct. Numerical simulations confirm effective task execution with solution times compatible with direct teleoperation of the arm.

2 Preliminaries

2.1 Kinematics

The HYRMAN's structure forms a 12-DoFs open kinematic chain made of a planar hyper-redundant arm and a dexterous 6-DoFs manipulator [4], as shown in Fig. 1, and whose DenavitHartenberg (DH) parameters are reported in Tab. 1.

[1] A Remote Handling Training Facility is being constructed at the CeSMA laboratory in the frame of Divertor Tokamak Test facility Upgrade (DTT-U) project by ENEA, in collaboration with DTT, CREATE (Consorzio di Ricerca per l'Energia, l'Automazione e le Tecnologie dell' Elettromagnetismo). The facility is equipped with a full-scale replica of a 110° sector of the DTT vacuum vessel.

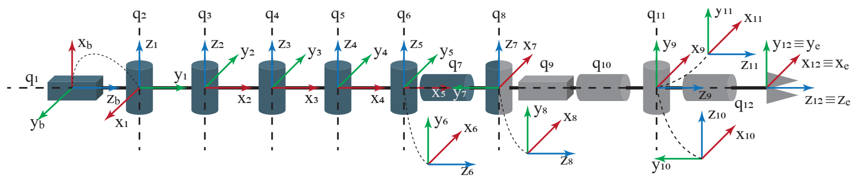

Fig. 1: HYRMAN kinematic chain with link frames, joint axes, and configuration variables $q_{1,\dots,12}$. The planar arm is highlighted with a blue shade.

Table 1: HYRMAN manipulator's Denavit-Hartenberg table.

Link	1	2	3	4	5	6	7	8	9	10	11	12
a	0	0.75	0.75	0.75	0.65	0	0	0	0	0	0	0
α	$\pi/2$	0	0	0	0	$\pi/2$	$-\pi/2$	$\pi/2$	0	$-\pi/2$	$\pi/2$	0
d	0	0	0	0	0	0	0.62	0	0	0	0	0.582
θ	$\pi/2$	0	0	0	0	0	0	0	0	0	0	0
offset	0	$\pi/2$	0	0	0	$\pi/2$	0	0	1.076	0	0	0

Let $\mathbf{q} \in \mathcal{Q} \subseteq \mathbb{R}^{12}$ denote the robot configuration vector, $\dot{\mathbf{q}}$ its time derivative, and let $\boldsymbol{\sigma} \in \mathcal{T} \subseteq \mathbb{R}^m$ be the task variable, where m is the task space dimension. Assuming that we can directly control the joint velocities, and that we can access the output $\boldsymbol{\sigma}$, the evolution of both the system and the task can be described as

$$\dot{\mathbf{q}} = \mathbf{u}, \quad \boldsymbol{\sigma} = \mathbf{k}(\mathbf{q}), \tag{1}$$

where $\mathbf{u} \in \mathcal{U} \subseteq \mathbb{R}^{12}$ is the control input, and $\mathbf{k}\colon \mathcal{Q} \to \mathcal{T}$ is a smooth map. Given the system model in (1), it follows that

$$\dot{\boldsymbol{\sigma}} = \mathbf{J}(\mathbf{q})\mathbf{u}, \tag{2}$$

where $\mathbf{J}\colon \mathcal{Q} \to \mathbb{R}^{m\times 12}$ is the task Jacobian defined as $\mathbf{J}(\mathbf{q}) = \frac{\partial \mathbf{k}}{\partial \mathbf{q}}(\mathbf{q})$ [7]. Equation (2) can be used to define the primary task and derive the joint velocities $\dot{\mathbf{q}}$ that achieve the desired end-effector Cartesian motion. However, as the robot is inherently redundant with respect to this task, other objectives can be executed in the Jacobians null space.

2.2 Extended Set-Based Tasks

In this work, objectives different from the end-effector motion, encoded with (2), are expressed as extended set-based (ESB) tasks [5], encompassing both tasks that enforce the state of the robot to remain in a given set (*forward invariance*), and tasks whose goal is to reach a desired set (*set stabilization*).

Examples of the former are joint-limit and collision avoidance, whereas the latter includes tasks such as pose regulation. More formally, we can define an ESB task as follows.

Definition 1 (ESB Task [5])

An ESB task is characterized by a set $\mathcal{C} \subset \mathcal{T}$*, where* $\mathcal{T}$ *is the task space, which can be expressed as the zero superlevel set of a continuously differentiable function* $h\colon \mathcal{T} \times \mathbb{R}_{\geq 0} \to \mathbb{R}$ *as* $\mathcal{C} = \{\boldsymbol{\sigma} \in \mathcal{T} \colon h(\boldsymbol{\sigma}, t) \geq 0\}$*. Executing the ESB task corresponds to rendering the time-varying set* $\mathcal{C}$ *forward invariant and asymptotically stable.*

The execution and satisfaction of ESB tasks can then be encoded in a control barrier function inequality constraint of an optimal control problem (OCP) [5]. Indeed, zeroing CBFs can induce a Lyapunov function and render sets asymptotically stable [1, 10], enabling the CBF formalism to encompass both safety and stabilization objectives. In the following, we show how prioritized ESB tasks execution can be exploited for our objective.

3 Method

The presented inverse kinematics approach is based on the solution of the following OCP, formulated as a QP:

$$\min_{\mathbf{u},\boldsymbol{\delta}} \|\mathbf{u}\|^2_{\mathbf{H}} + \|\boldsymbol{\delta}\|^2_{\mathbf{L}} \tag{3}$$

$$\text{s.t.} \quad \frac{\partial h_k}{\partial \boldsymbol{\sigma}_k} \frac{\partial \boldsymbol{\sigma}_k}{\partial \mathbf{q}} \mathbf{u} \geq -\gamma_k h_k(\boldsymbol{\sigma}_k) \qquad \forall\, k \in T_H, \tag{4}$$

$$\frac{\partial h_k}{\partial \boldsymbol{\sigma}_k} \frac{\partial \boldsymbol{\sigma}_k}{\partial \mathbf{q}} \mathbf{u} \geq -w_k(t, \boldsymbol{\sigma}_k)\gamma_k h_k(\boldsymbol{\sigma}_k) - \delta_k \qquad \forall\, k \in T_S, \tag{5}$$

$$\mathbf{J}(\mathbf{q})\mathbf{u} = \dot{\boldsymbol{\sigma}}_e \tag{6}$$

$$\mathbf{u}_{lb} \leq \mathbf{u} \leq \mathbf{u}_{ub}, \tag{7}$$

where $\boldsymbol{\sigma}_k$ contains the variables associated with the $k-$th task, h_k is the associated CBF, while $\dot{\boldsymbol{\sigma}}_e$ is the end-effector task velocity; T_H and T_S indicate the sets of hard and soft tasks, respectively; and $\boldsymbol{\delta}$ is the vector of slack variables. Moreover, $\|\cdot\|_H$ denotes a weighted norm, and $\mathbf{H} \in \mathbb{R}^{12\times 12}$ and $\mathbf{L} \in \mathbb{R}^{|T_s|\times|T_s|}$ are diagonal matrices. Equations (4) and (5) implement the CBF constraints for both set-based and secondary tasks using a linear class $\mathcal{K}^e_\infty$ function with constant gain $\gamma_k > 0$. Equation (6), where $\mathbf{J}(\mathbf{q})$ denotes the end-effector Jacobian, enforces satisfaction of the main task, while (7) specifies the input bounds $\mathbf{u}_{lb}$ and $\mathbf{u}_{ub}$. Finally, the function $w_k\colon \mathbb{R}_{\geq 0} \times \mathcal{T}_k \to [0, 1]$ is used to gradually activate a secondary task by increasing its gain over time, as better detailed in Sec. 3.2. This modification prevents jump discontinuities in the input; in fact, when $w_k = 0$ and $\dot{\boldsymbol{\sigma}}_e = 0$, the zero control input is the optimal solution, provided that the robot starts within the safe set defined by the hard-task barriers.

3.1 Hard tasks

The set of hard tasks T_H in (4) comprises safety-critical constraints that can not be violated, and includes:

1. Joint limits, which depend on the current robot configuration to allow the safe retraction of the planar arm through the duct. They are enforced using

$$h_i^+ = s_i(q_1, l_i)q_i^+ - q_i, \tag{8}$$

$$h_i^- = q_i - s_i(q_1, l_i)q_i^-, \quad \forall i = 1, \dots, 12, \tag{9}$$

$$s_i(q_1, l_i) = \begin{cases} \frac{1}{1+\exp(-\alpha(q_1+l_i))}, & \forall i = 2, 3, 4, 5, 6 \\ 1 & \text{otherwise} \end{cases} \tag{10}$$

where q_i^+ and q_i^- are the upper and lower limits for the $i-$th joint, respectively, α is a constant gain, and l_i is the $i-$th link displacement along the first joint axis, computed from the DH parameters. Therefore, setting $\boldsymbol{\sigma} = [q_1, q_i]^\mathsf{T}$ and using (4), the constraints are

$$-u_i + q_i^+ \alpha s_i(1 - s_i)u_1 \geq -\gamma_i h_i^+, \tag{11}$$

$$u_i - q_i^- \alpha s_i(1 - s_i)u_1 \geq -\gamma_i h_i^-. \tag{12}$$

Notice that (10), a sigmoid function used to reduce joint limits to zero when retracted, couples the $i-$th joint velocity with that of the first one, which governs the retraction speed. In addition, depending on the initial joint configuration, q_i^+ and q_i^- are modified to avoid singularity crossing.
2. Self-collision avoidance, implemented with the CBFs

$$h_{lm}^c = \|\mathbf{p}_l - \mathbf{p}_m\|^2 - d_{lm}^2, \quad \forall\, (l, m) \in \mathcal{C} \tag{13}$$

where $\mathbf{p}_l$ and $\mathbf{p}_m$ indicate two points on the robots' structure, $d_{lm} > 0$ is a minimum distance, and $\mathcal{C}$ is the set of link pairs for which the constraint is enforced. Thus, setting $\boldsymbol{\sigma}_{lm} = [\mathbf{p}_l^\mathsf{T}, \mathbf{p}_m^\mathsf{T}]^\mathsf{T}$, and substituting in (4), we have

$$2\left(\mathbf{p}_l - \mathbf{p}_m\right)^\mathsf{T} \left(\mathbf{J}_P^l(\mathbf{q}) - \mathbf{J}_P^m(\mathbf{q})\right)\mathbf{u} \geq -\gamma_{lm} h_{lm}^c, \tag{14}$$

having indicated with $\mathbf{J}_P^l$ and $\mathbf{J}_P^m$ the positional parts of the geometric Jacobian up to link l and m, respectively. Taking into account HYRMAN's joint limits, link geometries, and duct constraint, self-collisions can be avoided by imposing (14) among the 13 link pairs $\mathcal{C} = \{(1, 6), (2, 6), (1, 7),$

$(2,7),(3,7),(1,12),(2,12),(3,12),(4,12),(1,9),(2,9),(3,9),(4,9)\}$, and using the joint-frame positions for all links, except link 9, where the midpoint of the prismatic joint is employed.

3.2 Soft tasks

The set of soft tasks T_S, executed through (5), achieves secondary objectives within the null space of both the primary task (6) and the active constraints in (4) and (7). Since the application does not impose a strict priority order among them, a weighted approach is adopted; that is, the relative priority of these tasks can be tuned through the weights in $\mathbf{L}$. They are detailed in the following.

1. Maximize the distance from the Inner First Wall (IFW), realised by moving a set of links $\mathcal{L}_t$ to the middle of the tokamak torus, and implemented using the function

$$h_i^t = -\left((x_i - t_x)^2 + (y_i - t_y)^2 - r_t^2\right)^2, \quad \forall i \in \mathcal{L}_t \tag{15}$$

where x_i and y_i are the i-th link planar position, and t_x, t_y and r_t are the torus center coordinates and radius, respectively. This task should be active only for links that are inside the tokamak, for which $x_i > 0$ holds. Thus, w_i in (5) is used to avoid discontinuous velocities resulting from task activation, and is obtained by integrating

$$\dot{w}_i(t, x_i) = \begin{cases} 1/T & x_i \geq 0 \vee w_i < 1, \\ -1/T & x_i < 0 \vee w_i > 0, \\ 0 & \text{otherwise}, \end{cases} \tag{16}$$

initialized with $w_i = 0$, and where $T > 0$ is the insertion time interval. In this case, setting $\boldsymbol{\sigma}_i = [x_i, y_i]$, the constraint (5) becomes

$$-4\left((x_i - t_x)^2 + (y_i - t_y)^2 - r_t^2\right)[x_i - t_x, y_i - t_y, 0]\,\mathbf{J}_P(\mathbf{q})\mathbf{u} \geq -w_i\gamma_i h_i^t - \delta_i.$$

2. Minimize the torque on Joint 7, which is critical due to its reduced limits, compared to the other joints, and the need to carry high payloads at the end effector. This task can be executed by generating joint velocities that drive the following CBF to zero

$$h^{\tau_7} = -\left\{\mathbf{J}_{10}(\mathbf{q})\right\}_{3,7}^2 = -\left((q_9 + q_9^o)\cos(q_7)\sin(q_8)\right)^2, \tag{17}$$

where $\{\cdot\}_{3,7}$ indicates the element in position $(3,7)$, and q_9^o is the offset on joint 9. Posing $(q_9 + q_9^o)\cos(q_7)\sin(q_8) := g$, constraint (5) becomes

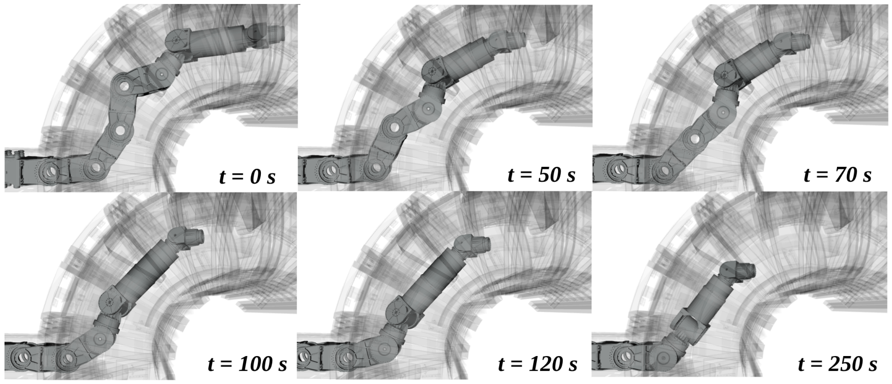

Fig. 2: Sequence of robot configurations along the trajectory, progressing from the upper left to the lower right. The tokamak is depicted in shaded grey.

$$-2g\frac{\partial g}{\partial \mathbf{q}}\mathbf{u} \geq -w(t)\gamma h^{\tau_7} - \delta, \tag{18}$$

where $w(t) = \min(T^{-1}t, 1)$ is used to gradually insert the task in the stack.

3. Minimize the planar arm length within the vessel, which can be achieved by minimizing the extension of the first prismatic joint with the function

$$h^{j_1} = -(q_1 - q_1^-)^2. \tag{19}$$

As $\boldsymbol{\sigma} = q_1$, the task can be executed by imposing

$$-2(q_1 - q_1^-)u_1 \geq -w(t)\gamma h^{j_1} - \delta, \tag{20}$$

and employing the same function $w(t)$ of the previous task.

4 Results

This section presents the results obtained by applying the proposed method in a numerical simulation. More in detail, the task of minimizing the distance from the toroidal center is applied to the set of links $\mathcal{L}_t = \{3, 4, 5, 8\}$. The input limits are $u_{\mathrm{ub}} = 0.035$ rad/s for revolute joints and $u_{\mathrm{ub}} = 0.05$ m/s for prismatic ones, with $u_{\mathrm{lb}} = -u_{\mathrm{ub}}$. The weights in the cost function are $\mathbf{H} = 100\mathbf{I}_{12}$, $\mathbf{L} = 50\mathbf{I}_6$. In constraint (6), the desired task space velocity is given by $\dot{\boldsymbol{\sigma}}_e = [(\dot{\mathbf{p}}_d + \mathbf{K}_P\mathbf{e}_P)^\mathsf{T},\ (\boldsymbol{\omega}_d + \mathbf{K}_O\mathbf{e}_O)^\mathsf{T}]^\mathsf{T}$ with $\mathbf{K}_P = 10\,\mathbf{I}_3$, $\mathbf{K}_O = 6.5\,\mathbf{I}_3$, and where $\mathbf{e}_P$ is the position error and $\mathbf{e}_O$ is the orientation error computed as in [7]. Enforcing all tasks results in an optimization problem with 18 decision variables and 73 constraints, which was solved on a standard laptop using

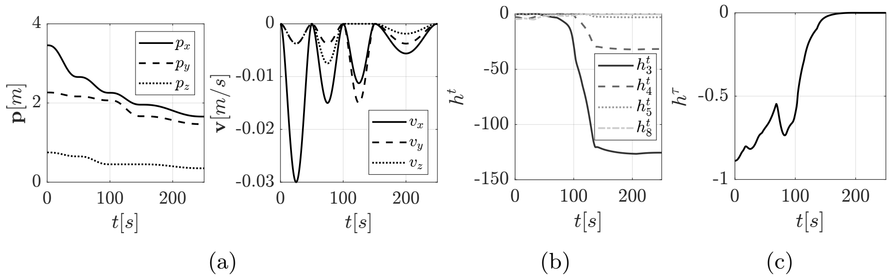

Fig. 3: (a) End-effector desired position and linear velocity. (b) Time evolutions of the task moving links to the torus center. (c) Time evolution of h^{τ_7}.

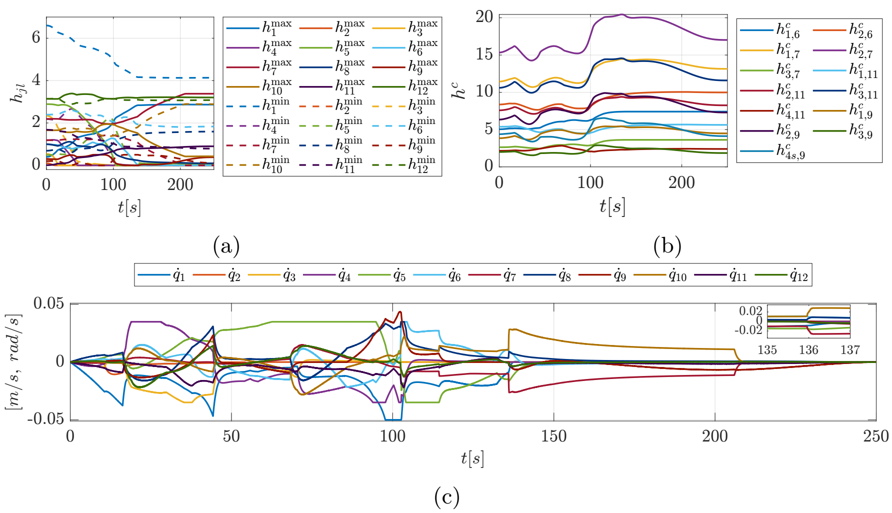

Fig. 4: (a) Time evolution of the CBFs for joint limits enforcement. (b) Time evolution of the CBFs for self-collision avoidance. (c) Joint velocities computed solving QP (3). The zoomed plot shows the inputs continuity around $t = 136$ s.

the OSQP library [8] with sampling time $dt = 0.01$ s. Figure 2 depicts the initial, intermediate, and final configurations of HYRMAN inside the vessel, with the planar joints positions converging to zero while the arm retracts in the duct. The desired end-effector trajectory is a sequence of five rectilinear segments with constant orientation, and its position profile is depicted in Fig. 3a. Figures 3b and 3c show the time evolution of the soft tasks functions h^t and h^{τ_7}. As these tasks are lower in priority and therefore relaxed, their values may remain negative; nevertheless, the torque on joint 7 converges to zero in the final configuration (see also the lower-right image in Fig. 2). Figures 4a and 4b depict the hard barrier values corresponding to joint limits and self-collision, respectively. These functions remain positive, indicating that all safety constraints are satisfied. Finally, Figure 4c plots the optimized joint velocities, with saturation occurring due to input limits. In the reported scenario, we obtained a mean solution time of $\mu = 6.75 \times 10^{-5}$ s with standard deviation $\sigma = 1.7 \times 10^{-5}$ s, indicating that the approach is suitable both for offline trajectory inversion and for direct teleoperation.

5 Conclusions

In this paper, we presented an optimization-based approach to solve the inverse kinematics of a hyper-redundant manipulator for nuclear plant maintenance. We formulated a quadratic optimization problem, encoding safety and secondary tasks as inequality constraints. Simulations indicate that the method can address some of the challenges posed by maneuvering the robot in the vessels confined space, particularly at the duct entrance, and that the problem can be efficiently solved online.

Acknowledgements This study was supported by ENEA in the context of the DTT-U project, involving Universitá di Napoli Federico II, OCIMA s.r.l., and ENI/Eniprogetti, by the INVITALIA Project NEMESI - CUP C67G22000420008, and by the SPACE IT UP project, financed by the Italian Space Agency (ASI) and by the Ministry of University and Research (MUR), with contract no. 2024-5-E.0 - CUP n. I53D24000060005.

References

1. Ames, A.D., Coogan, S., Egerstedt, M., Notomista, G., Sreenath, K., Tabuada, P.: Control barrier functions: Theory and applications. In: 2019 18th European Control Conference (ECC), pp. 3420–3431 (2019)
2. Capodivento, L., Borzone, T., Grasso, T., Lauretti, C.: A bidirectional human-machine control interface based on virtual fixtures for safe teleoperation of hyper-redundant robots. IEEE Access (2024)
3. Chiaverini, S., Oriolo, G., Maciejewski, A.A.: Redundant robots. In: B. Siciliano, O. Khatib (eds.) Springer Handbook of Robotics, pp. 221–242. Springer International Publishing, Cham (2016)
4. Lauretti, C., Grasso, T., de Marchi, E., Grazioso, S., di Gironimo, G.: A geometric approach to inverse kinematics of hyper-redundant manipulators for tokamaks maintenance. Mechanism and Machine Theory **176**, 104,967 (2022)
5. Notomista, G., Mayya, S., Selvaggio, M., Santos, M., Secchi, C.: A set-theoretic approach to multi-task execution and prioritization. In: 2020 IEEE International Conference on Robotics and Automation (ICRA), pp. 9873–9879. IEEE (2020)
6. Sciavicco, L., Siciliano, B.: A solution algorithm to the inverse kinematic problem for redundant manipulators. IEEE Journal on Robotics and Automation **4**(4), 403–410 (1988)
7. Siciliano, B., Villani, L., Oriolo, G., De Luca, A., et al.: Foundations of robotics. Advanced Textbooks in Control and Signal Processing (2025)

8. Stellato, B., Banjac, G., Goulart, P., Bemporad, A., Boyd, S.: OSQP: an operator splitting solver for quadratic programs. Mathematical Programming Computation **12**(4), 637–672 (2020)
9. Wang, H., Lai, Y., Chen, W., Cao, Q.: Design and implementation of motion planning of inspection and maintenance robot for iter-like vessel. Fusion engineering and design **101**, 111–123 (2015)
10. Xu, X., Tabuada, P., Grizzle, J.W., Ames, A.D.: Robustness of control barrier functions for safety critical control. IFAC-PapersOnLine **48**(27), 54–61 (2015)